Highly Sensitive DNA Sensor Based on Upconversion Nanoparticles and Graphene Oxide

P. Alonso-Cristobal,[†] P. Vilela,[§] A. El-Sagheer,[‡] E. Lopez-Cabarcos,[†] T. Brown,[‡] O. L. Muskens,[§] J. Rubio-Retama,*[,†] and A. G. Kanaras*[,§]

[†]Department of Physical Chemistry II, Faculty of Pharmacy, Complutense University of Madrid, 28040 Madrid, Spain

[‡]Department of Chemistry, University of OxfordChemistry Research Laboratory, Oxford OX1 3TA, United Kingdom

[§]Institute for Life Sciences, Physics and Astronomy, Faculty of Physical Sciences and Engineering, University of Southampton, Southampton SO17 1BJ, United Kingdom

Ⓢ Supporting Information

ABSTRACT: In this work we demonstrate a DNA biosensor based on fluorescence resonance energy transfer (FRET) between $NaYF_4$:Yb,Er nanoparticles and graphene oxide (GO). Monodisperse $NaYF_4$:Yb,Er nanoparticles with a mean diameter of 29.1 ± 2.2 nm were synthesized and coated with a SiO_2 shell of 11 nm, which allowed the attachment of single strands of DNA. When these DNA-functionalized $NaYF_4$:Yb,Er@SiO_2 nanoparticles were in the proximity of the GO surface, the $\pi-\pi$ stacking interaction between the nucleobases of the DNA and the sp^2 carbons of the GO induced a FRET fluorescence quenching due to the overlap of the fluorescence emission of the $NaYF_4$:Yb,Er@SiO_2 and the absorption spectrum of GO. By contrast, in the presence of the complementary DNA strands, the hybridization leads to double-stranded DNA that does not interact with the GO surface, and thus the $NaYF4$:Yb,Er@SiO_2 nanoparticles remain unquenched and fluorescent. The high sensitivity and specificity of this sensor introduces a new method for the detection of DNA with a detection limit of 5 pM.

KEYWORDS: upconversion nanoparticles, graphene oxide, FRET, DNA biosensor
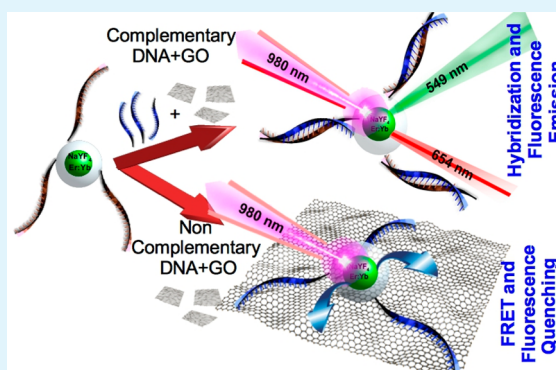
INTRODUCTION

DNA is a biopolymer that can self-assemble in a unique manner according to the Watson—Crick base pairing rules. This self-assembly between two complementary polymer chains, known as hybridization, is very specific and is based on the cooperative hydrogen bonds produced between the base pairs, rendering a double-helix structure. The DNA base-pair complementarity has shown great potential in nanotechnology as a structural material in DNA origami,[1] polyhedral structures,[2] nanomechanical devices,[3] and as a template for the self-assembly of other materials such as gold nanoparticles.[4−6] This hybridization process has also been of great potential in biomedicine for applications in sensors.[7] The specificity of the self-assembly between complementary DNA strands can be employed for the detection of certain sequences of interest, which are related to viral[8] or bacterial[9] infections as well as in the detection of specific human DNA or mRNA sequences for the diagnosis of diseases[10] or mutations.[11]

Biosensors based on controlled quenching of fluorescence labels have shown significant advantages when employed as molecular beacons for amplified detection of metal ions and organic molecules.[12−14] Such sensors are typically designed with an energy transfer pair in which the fluorescence of the donor is effectively quenched by the acceptor. The addition of complementary target DNA or RNA induces a separation between the donor and the acceptor, and consequently the fluorescence of the donor is turned on proportionally to the concentration of the target. The sensing of DNA using these assays is often based on a self-complementary sequence within a hairpin loop that creates an intimate contact between the quencher and the fluorescent dye. Upon the addition of the complementary DNA, the hybridization results in a separation of the fluorophore from the quencher and the fluorescence can be detected.[15−17] Other assays can detect the activity of DNAase enzymes, which can selectively cleave a specific oligonucleotide sequence, thus separating the fluorophore from the quencher and restoring the fluorescence.[18] Although there are many strategies for the design of DNA-based sensors, the detection sensitivity is determined by the fluorophores. The commonly used organic dyes suffer from photobleaching, while

inorganic quantum dots exhibit blinking effects. However, the main drawback is the excitation wavelength of these fluorophores, which is normally located in the UV−vis region. Furthermore, the fluorescence background originating from biomolecules[19] and the inner filter effect provoked by the absorption of other species[20] limit the detection sensitivity.

These drawbacks could be overcome using upconversion nanoparticles (UCNPs) as fluorescence donors.[21] The UCNPs are lanthanide-doped inorganic materials, which are able to absorb two or more low-energy photons and emit fluorescence at a shorter wavelength than the excitation wavelength.[22] It is important to note that the upconversion fluorescence is produced by the inner 4f−4f orbital electronic transitions that are shielded by the complete 5s and 5p orbitals.

They have shown several advantages as fluorescence probes due to their high chemical and photochemical stability, low toxicity, large Stokes shifts, lack of photobleaching, and absence of blinking. For these advantages, the UCNPs have been used in different applications.[23−28] However, the most important feature that makes the UCNPs an alternative to classical organic dyes is the excitation wavelength, which is located in the near-infrared (NIR) region (typically 980 nm). At this excitation wavelength biomolecular autofluorescence is avoided, while obtaining a lower light scattering when compared with UV−vis radiation.[29] For these reasons, the signal-to-noise ratio can be greatly enhanced by using UCNPs as biological labels,[30] and the quenching of this fluorescence is only possible on the surface of the particles.[31] For this reason, the upconversion fluorescence would require nanoparticles in which the surface-related effects are dominant. Thus, an effective quencher for upconversion fluorescence is difficult to find.[32] Among other quenchers,[33,34] water-soluble graphene oxide (GO) has been used as an ultra-highly efficient quencher for UCNPs, when the nanoparticles are in intimate contact with the GO surface.[35] For this to happen, it would be necessary to functionalize the UCNPs with molecules capable of physisorbing onto the GO surface. It has been demonstrated that single-strand DNA (ssDNA) biopolymers have a strong affinity for the surface of GO due to strongly attractive π−π interactions between the aromatic nucleobases and the highly unsaturated structure of GO.[36] In contrast, in the case of double-stranded (dsDNA) π-electrons are involved in forming the duplex via base-stacking interactions. Thus, they are not available for interactions with the GO surface. On this basis, it would be possible to design a fluorescence sensor for DNA using UCNPs and GO as a fluorescence resonance energy transfer (FRET) pair. Such upconversion fluorescence probes would be functionalized with ssDNA and should be highly monodisperse and small enough to permit FRET with GO. In the presence of the complementary DNA strand (cDNA) the hybridization process would lead to dsDNA, and the upconversion fluorescence would be detectable.

In this work a fluorescence DNA sensor platform is demonstrated using the FRET pair formed by UCNPs as fluorophores and GO as quencher. Erbium- and ytterbium-doped β-NaYF$_4$ nanoparticles were used as fluorescent donors, which are known as one of the most efficient upconverting nanomaterials.[37] The ratio between the ssDNA-functionalized UCNPs and GO was optimized to obtain the maximum sensitivity, and the biosensor was evaluated using the cDNA sequence at different concentrations. In addition, the hybridization conditions of the DNA sequences were studied as a function of temperature. A strong relationship was found

between these conditions and the sensitivity of the sensor. By using relative emission/upconversion measurements compared to a reference, it was possible to determine the presence of cDNA with a great sensitivity and specificity with a fast and reproducible methodology.

■ EXPERIMENTAL SECTION

Materials. Erbium(III) chloride hexahydrate (99.9%), ytterbium-(III) chloride hexahydrate (99.9%), yttrium(III) chloride hexahydrate (99.99%), 1-octadecene (80%), oleic acid (90%), sodium hydroxide (98%), ammonium fluoride (98%), methanol (99.9%), n-hexane (95%), N,N-dimethylformamide anhydrous (DMF) (99.8%), tetraethyl orthosilicate (TEOS) (99.999%), polyoxyethylene (5) non-ylphenylether, branched (IGEPAL CO-520), ammonium hydroxide solution (30%), (3-aminopropyl)triethoxysilane (APTES) (99%), succinic anhydride (99%), phosphate-buffered saline (PBS) tablets, N-(3-(dimethylamino)propyl)-N′-ethylcarbodiimide hydrochloride (EDC) (99%), and N-hydroxysulfosuccinimide sodium salt (Sulfo-NHS) (98%) were purchased from Sigma-Aldrich (St. Louis, MO) and used as received. GO (powder) was purchased from Graphene Supermarket, Inc. (New York, NY). The PBS solutions were prepared dissolving the tablet following the manufacturer's specifications.

The DNA sequences were synthesized by the Brown group (School of Chemistry, University of Oxford, U.K.). The ssDNA probe sequence that was covalently linked to the surface of the nanoparticles was 5′-aminohexyl-TTTTTTTTTTTTTTTTTTTTTTTT-3′. The cDNA sequence (was 5′-AAAAAAAAAAAAAAAA−AAAAAAAAAAAAAAAA-3′. The random sequence (noncomplementary ssDNA sequence) was 5′-CTAGATCCGTGTCCTCGT-3′. All the DNA oligomers were purified by reversed-phase HPLC, and the concentration was calculated with UV−vis spectroscopy.

Synthesis of Monodisperse NaYF$_4$:Yb,Er Nanoparticles. The synthesis was performed by following a previously reported procedure[38,39] with slight modifications yttrium(III) chloride hexahydrate (236.62 mg, 0.78 mmol), ytterbium(III) chloride hexahydrate (77.5 mg, 0.20 mmol), and erbium(III) chloride hexahydrate (7.63 mg, 0.02 mmol) were dissolved in a three-necked round-bottom flask with oleic acid (6 mL, 19 mmol) and 1-octadecene (15 mL, 46.9 mmol) and heated at 160 °C for 1 h and 30 min under nitrogen atmosphere. After this time, a solution of sodium hydroxide (100 mg, 2.5 mmol) and ammonium fluoride (148.16 mg, 4 mmol) dissolved in 10 mL of methanol was added dropwise in the reaction under vigorous stirring. This mixture was slowly heated to 100 °C for 2 h under nitrogen atmosphere and then 30 more minutes under vacuum. Next, the flask containing the mixture was set up with a thermometer, a reflux condenser, and nitrogen atmosphere and was placed in a heating mantle. The temperature was raised to 300 °C and left to react for 1 h and 30 min. Subsequently, the mixture was left to cool to room temperature, and the NaYF$_4$:Yb,Er nanoparticles were collected by centrifugation (8500 rpm, 10 min) with a mixture of hexane, ethanol, and water (2:1:1 v/v). The pellet was redispersed with 5 mL of ethanol and centrifuged in a mixture of ethanol and water (1:1 v/v). This process was repeated three times. Finally, the purified NaYF$_4$:Yb,Er nanoparticles were redispersed and stored in hexane. The Supporting Information, Figure S6 shows the EDS spectrum, which reveals the atomic composition of the nanoparticles.

Synthesis of NaYF$_4$:Yb,Er@SiO$_2$ Nanoparticles. The silica coating of the synthesized UCNPs was achieved by the base-catalyzed polymerization of TEOS in a reverse microemulsion.[40,41] Briefly, 240 mg of IGEPAL CO-520 and 5 mL of a hexane solution with the UCNPs (2 mg/mL) were mixed with an ultrasound bath. Then, ammonium hydroxide solution (40 μL, 30%) was added and gently mixed. The solution turned totally transparent, which indicated the formation of the microemulsion. The reaction started when TEOS (30 μL, 0.14 mmol) was added under stirring, and it was left to react overnight at room temperature. The reaction finished when the microemulsion was destabilized with 5 mL of methanol. The core@shell NaYF$_4$:Yb,Er@SiO$_2$ nanoparticles (UCNPs@SiO$_2$) were purified by centrifugation (3 × 8500 rpm, 10 min) with ethanol. The
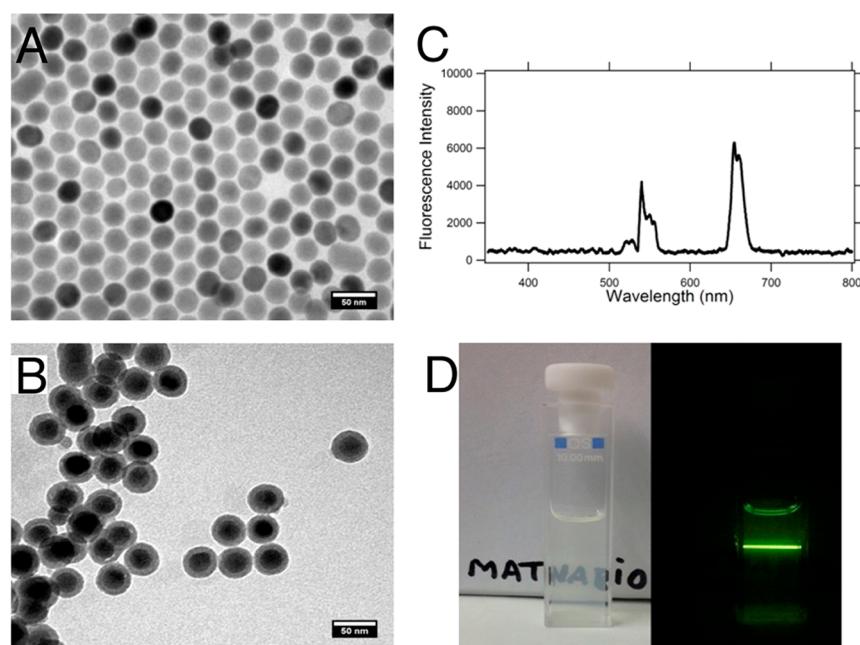
Figure 1. (A) TEM micrograph of monodisperse NaYF$_4$:Yb,Er nanoparticles. (B) TEM micrograph of monodisperse and individually coated NaYF$_4$:Yb,Er@SiO$_2$ nanoparticles. Scale bars are 50 nm. (C) Fluorescence spectrum of a diluted solution in ethanol of the silanized upconversion nanoparticles when excited with a continuous wave 980 nm laser. (D) Pictures taken of the diluted solution of silanized upconversion nanoparticles in ethanol without laser excitation (left) and the same solution under the excitation of a cw 980 nm laser (right). The room light was turned off to take this picture.

Supporting Information, Figure S7 shows the FTIR spectrum of the obtained nanoparticles.

Surface Modification of the NaYF$_4$:Yb,Er@SiO$_2$ Nanoparticles. The carboxylic acid-functionalized NaYF$_4$:Yb,Er@SiO$_2$ nanoparticles (UCNPs@SiO$_2$−COOH) were prepared by sequential functionalization steps.[42] First, the surface was functionalized with amino groups by the addition of APTES (150 μL, 0.68 mmol) to the synthesized UCNPs@SiO$_2$ dissolved in 5 mL of ethanol. This mixture was stirred at room temperature overnight. The UCNPs@SiO$_2$−NH$_2$ nanoparticles were centrifuged (3×) and dispersed in 5 mL of anhydrous DMF. Then, succinic anhydride (150 mg, 1.49 mmol) was dissolved in 3 mL of anhydrous DMF, added dropwise to the anhydrous DMF solution containing the UCNPs@SiO$_2$−NH$_2$, and stirred at room temperature overnight. The ring-opening reaction led to the carboxylic acid-functionalized upconversion@silica nanoparticles, which were collected by centrifugation. The DMF solvent traces were removed after several centrifugation steps with ethanol. Finally, the UCNPs@SiO$_2$−COOH nanoparticles were dispersed in water.

Attachment of the Probe ssDNA Sequence to the NaYF$_4$:Yb,Er@SiO$_2$ Nanoparticles. The DNA was covalently attached to the surface of the nanoparticles by the carbodiimide coupling reaction. This reaction produced a covalent bond between the carboxylic acid group on the surface of the UCNPs@SiO$_2$ nanoparticles and the amino group in the 5′ end of the probe ssDNA sequence. The EDC coupling reaction was performed as follows: The UCNPs@SiO$_2$−COOH nanoparticles were dispersed in a borate-buffered solution (0.001 M) at a concentration of 1.82 mg/mL. This solution (200 μL, 0.364 mg of nanoparticles) was added to an eppendorf tube prior to the addition of an EDC solution in borate buffer (20 μL, 0.3 M) and a Sulfo-NHS solution in borate buffer (40 μL, 0.3 M). The mixture was shaken for 5 min, and then the aqueous solution of probe ssDNA (30 μL, 220.65 μM) was added. The reaction was stirred overnight, and the probe ssDNA-functionalized nanoparticles (UCNPs@SiO$_2$-ssDNA) were purified by centrifugation (16 400 rpm, 20 min) twice. The purified UCNPs@SiO$_2$-ssDNA nanoparticles were collected with PBS solution (0.01 M, pH 7.4) and stored at −20 °C.

Characterization Methods. Transmission electron microscopy (TEM) specimens of the nanoparticles were prepared by placing a drop of a diluted solution on a TEM copper grid coated with a Formvar film and left to dry in air. The size and morphology of the samples were observed with a JEM-1010 electron microscope working at 80 kV equipped with a digital camera GATAN megaview II (JEOL, Japan). The nanoparticle size distribution was analyzed with ImageJ (National Institutes of Health, USA) and Soft Imaging Viewer (Olympus, Japan) software, considering over 300 nanoparticles for the statistical analysis. The upconversion fluorescence measurements were performed in a manually aligned setup with a continuous wave 980 nm 500 mW diode laser (Armlaser, USA) as excitation source and a SpectraSuite Spectrometer (OceanOptics, USA) as detector. The detector was placed at an angle of 90° to the excitation beam, and the emitted fluorescence was collected via fiber-optic cable and measured with the software provided by SpectraSuite (OceanOptics, USA). A cuvette with the corresponding solvent was measured under illumination with the 980 nm laser beam and set as the blank for each measurement. All measurements were performed with 2.000 ms of integration time and 100 scans to average. All fluorescence experiments were repeated at least three times with independent measurements, and the fitted data presented in this manuscript shows the statistically significant mean value ± error. The represented data (graphs) represent one individual measurement for an easier visualization. The Z-potential measurements were performed using a Zetasizer Nano ZS instrument (Malvern Instruments, U.K.), and the accumulation time was determined automatically for each sample. The acquired data was processed using the software provided by Malvern (Zetasizer software v7.03).

■ RESULTS AND DISCUSSION

Synthesis and Surface Functionalization of Upconversion Nanoparticles. The synthesis of NaYF$_4$:Yb,Er nanoparticles produced highly monodisperse spherical UCNPs with a mean diameter of 29.1 ± 2.2 nm as measured by TEM micrographs (Figure 1A). These nanoparticles could be easily dispersed in organic solvents such as hexane due to

Scheme 1. A Schematic Illustration of the Chemical Route for the Functionalization of UCNPs@SiO$_2$ Nanoparticles[a]
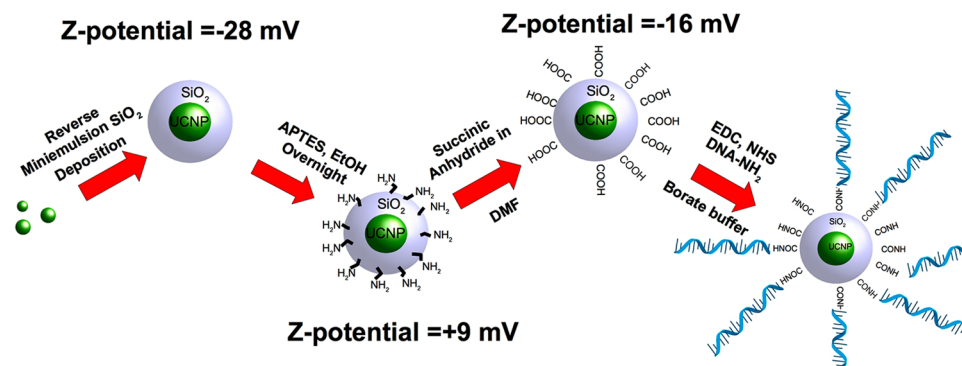
[a]The first experimental step was the silanization of the upconversion nanoparticles. Then, the surface was modified with amino groups using APTES. These amino groups acted as nucleophiles for the reaction with succinic anhydride, which led to carboxylic acid-functionalized UCNPs@SiO$_2$ nanoparticles. The final experimental step was the EDC coupling reaction between the amino-modified probe ssDNA sequence and the obtained carboxylic acid in the surface of the nanoparticles.

the presence of oleic acid as capping and stabilizing agent. The UCNPs were subsequently coated with a silica shell by a reverse microemulsion method. With this procedure it was possible to obtain monodisperse spherical core@shell NaYF$_4$:Yb,Er@SiO$_2$ nanoparticles in which each upconversion nanoparticle was covered with silica, and no large aggregates with multiple-core were found. The overall mean diameter of the UCNPs@SiO$_2$ nanoparticles was 47.34 $\pm$ 3.8 nm with a silica shell thickness of $\sim$11 nm as analyzed with TEM micrographs (Figure 1B). The UCNPs@SiO$_2$ nanoparticles could be dispersed in polar solvents such as ethanol or water. The obtained nanoparticles showed the characteristic upconversion fluorescence spectrum for ytterbium- and erbium-doped NaYF$_4$ nanoparticles when excited with a CW 980 nm 500 mW laser diode (Figure 1C). The upconversion fluorescence with these erbium-doped nanoparticles showed the emissions at 534 and 549 nm (green emission corresponding to the transition $^4S_{3/2} \rightarrow \ ^4I_{15/2}$) and at 654 nm (red emission corresponding to the transition $^4F_{9/2} \rightarrow \ ^4I_{15/2}$).[43] The quantum efficiency of particles having the same size, composition, and structure is $\sim$0.1%.[44] The nanoparticles dispersed in water formed a transparent solution in which the upconversion fluorescence could be observed by the naked eye when the sample was excited with the 980 nm laser (Figure 1D). The surface of the NaYF$_4$:Yb,Er@SiO$_2$ nanoparticles was modified in several steps prior to the covalent attachment of the ssDNA sequence (Scheme 1).

The first experimental step was the addition of an excess of APTES to the nanoparticles in ethanol. The Z-potential of the UCNPs@SiO$_2$ nanoparticles turned from -28.3 ± 3.55 mV to $+8.74 \pm 3.99$ mV, which was indicative of the presence of NH$_2$ groups on the surface of the nanoparticles (named UCNPs@SiO$_2$–NH$_2$). The variation of the Z-potential was concomitant with a reduction of the aqueous stability of these nanoparticles. This step provided amino groups, which could act as nucleophilic centers for the reaction with succinic anhydride in DMF. This ring-opening reaction created a covalent amide bond and a terminal carboxylic acid group in the surface of the nanoparticles. After the reaction, the Z-potential changed from $+8.74 \pm 3.99$ mV to -16.4 ± 3.99 mV indicating the presence of carboxylate groups. The resulting UCNPs@SiO$_2$–COOH nanoparticles were highly stable in aqueous solution. Figure 2 shows the Z-potential of the UCNPs@SiO$_2$, UCNPs@SiO$_2$–NH$_2$ and UCNPs@SiO$_2$–COOH nanoparticles, respectively.
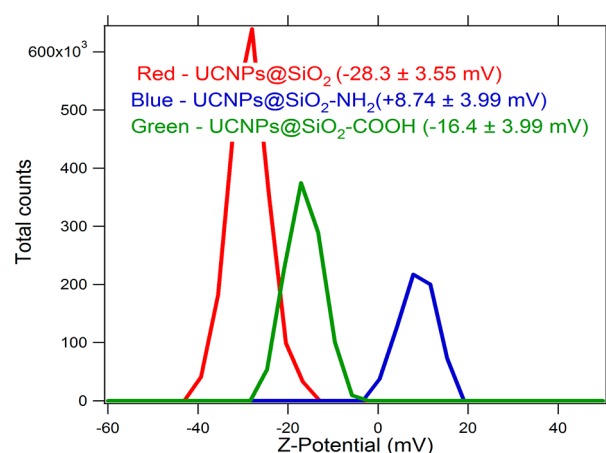

Figure 2. Z-potential measurements of the surface-functionalized upconversion nanoparticles: UCNPs@SiO$_2$ nanoparticles (red curve); UCNPs@SiO$_2$–NH$_2$ nanoparticles (blue curve); and UCNPs@SiO$_2$–COOH nanoparticles (green curve).

The presence of carboxylic groups on the surface of the UCNPs@SiO$_2$–COOH allows to covalently attach amine-modified ssDNA utilizing the EDC/sulfo-NHS coupling reaction. The amine-modified probe ssDNA was used in excess in the synthesis as previously reported for other systems.[45]

Optimization and Evaluation of the ssDNA Sensor Based on UCNPs and Graphene Oxide. The FRET pair between UCNPs@SiO$_2$-ssDNA and GO was studied for the optimization of the sensor. First, the concentration of UCNPs@SiO$_2$-ssDNA nanoparticles was set to 0.4 mg/mL. Different concentrations of GO (ranging from 0 to 1 mg/mL) were prepared and incubated with the nanoparticles at 40 °C for 1 h. Then, the samples were left to cool to room temperature prior to the fluorescence measurements.

Figure 3 depicts the reduction of fluorescence intensity of UCNPs@SiO$_2$-ssDNA (0.4 mg/mL) when the concentration of GO increased. The analysis of the fluorescence quenching of UCNPs@SiO$_2$-ssDNA nanoparticles at 549 and 654 nm as a function of the GO concentration is shown in Figure 4. Figure 4a shows the absolute intensity, while Figure 4b shows the same data normalized to the value without GO.

Clearly, the fluorescence intensity was quenched by more than 95% when the concentration of GO reached $\sim$0.3 mg/mL.
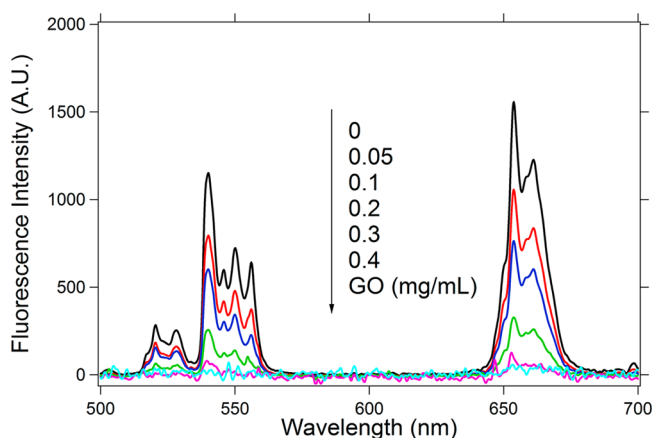
Figure 3. Upconversion fluorescence spectra of the UCNPs@SiO₂-ssDNA nanoparticles (0.4 mg/mL) in the presence of different concentrations of graphene oxide (excitation wavelength 980 nm). Higher concentrations of GO result in reduced upconversion intensity.
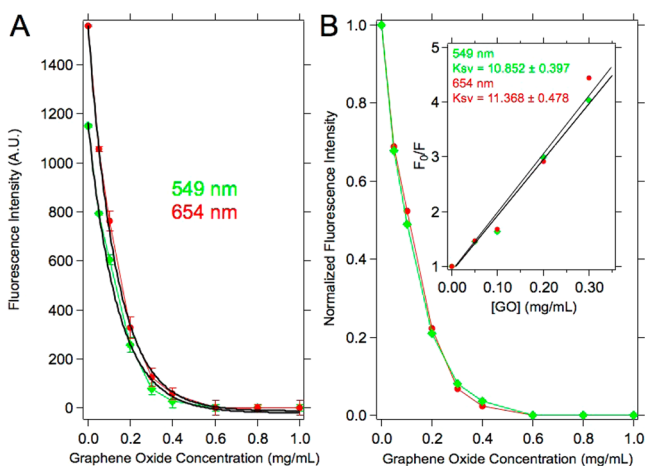

Figure 4. Representation of (A) the maximum fluorescence intensity and (B) normalized fluorescence intensity of the UCNPs@SiO₂-ssDNA (0.4 mg/mL) measured at 549 and 654 nm as a function of the GO concentration. (inset) The Stern−Volmer plot for the fluorescence quenching with GO of the emission bands located at 549 nm (green line) and 654 nm (red line).

A further addition of GO resulted only in a very small increase in quenching. As shown in Figure 4b, this behavior was similar for both nanoparticle emission wavelengths located at 549 and 654 nm. These observations led us to hypothesize 0.3 mg/mL of GO as the optimum concentration for quenching the fluorescence emission of 0.4 mg/mL of the UCNPs@SiO₂-ssDNA.

A quantitative measure of the fluorescence quenching is given by the Stern−Volmer constant K_{SV}, defined by the following equation:

$$F_0/F = 1 + K_{sv}\cdot[GO]$$

where F_0 and F are the intensities of fluorescence in the absence and in the presence of the quencher, respectively, and $[GO]$ is the concentration of quencher. For the UCNPs@SiO₂-ssDNA quenched by GO the obtained K_{sv} value was ~11 mL/mg for both wavelengths, indicating that the quenching mechanism was due to FRET between the UCNPs and the GO and not by a simple absorption process in which the GO would absorb the photons emitted by the UCNPs. If this was the case, the

fluorescence quenching of the photons at 549 nm would have been higher than that of the photons at 654 nm, due to the absorption spectrum of GO (Figure S2 in the Supporting Information).

With the aim of assessing the importance of the interaction between the ssDNA and GO on the fluorescence quenching of the UCNPs@SiO₂-ssDNA, we compared the fluorescence of UCNPs@SiO₂ with and without ssDNA at a concentration of 0.4 mg/mL; see Figure 5.
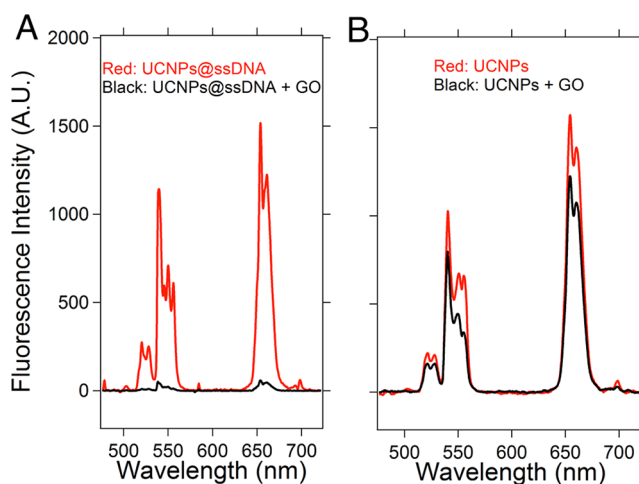

Figure 5. (A) Fluorescence intensity of 0.4 mg/mL of UCNPs@SiO₂-ssDNA nanoparticles in the presence (black curve) and in the absence (red curve) of 0.3 mg/mL of GO. (B) Fluorescence intensity of 0.4 mg/mL of UCNPs@SiO₂ nanoparticles in the presence (black curve) and in the absence (red curve) of 0.3 mg/mL of GO. Both samples were incubated for 1 h at 40 °C.

The Figure 5A,B reveals the differences of the fluorescence quenching observed on UCNPs@SiO₂ nanoparticles with and without DNA, respectively. These results demonstrated that the FRET-based fluorescence quenching was specific for UCNPs@SiO₂-ssDNA nanoparticles and was due to the attractive π−π interactions between the ssDNA and the GO surface.

A means to disrupt the attractive π−π interactions between the ssDNA and the GO surface could be hybridization of the ssDNA strand with its complementary ssDNA sequence. This would induce a conformational change of the DNA strands that would prevent the adsorption of the UCNPs@SiO₂-ssDNA nanoparticles on the GO surface. As a result, the UCNPs@SiO₂-ssDNA nanoparticles would retain their fluorescence. To prove this, 0.4 mg/mL of UCNPs@SiO₂-ssDNA nanoparticles were incubated in PBS with different concentrations of the complementary ssDNA (from 0.1 nM to 400 nM) for 2 min at 90 °C and then slowly cooled to 40 °C. After this time, a solution of GO in PBS was added to make a final concentration of 0.3 mg/mL. The mixture was incubated for 1 h at 40 °C and then cooled to room temperature prior to performing the fluorescence measurements. Figure 6 represents the fluorescence intensity of UCNPs@SiO₂-ssDNA nanoparticles in the presence of GO and different concentrations of the complementary ssDNA.

The fluorescence intensity of the UCNPs@SiO2-ssDNA nanoparticles shows a gradual recovery with increasing concentrations of the complementary ssDNA. The analysis of the maximum intensity as a function of the concentration of the
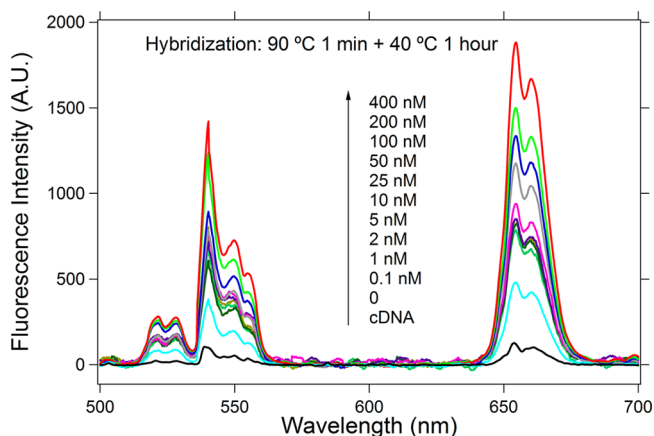
Figure 6. Representation of the fluorescence spectra of the UCNPs@SiO$_2$-ssDNA nanoparticles (0.4 mg/mL) in the presence of different concentrations of complementary ssDNA and 0.3 mg/mL of GO (red curves). The black curve is the fluorescence spectrum without the addition of complementary ssDNA (excitation at 980 nm).

complementary ssDNA is presented in Figure 7 for the two upconversion wavelengths at 549 and 654 nm.
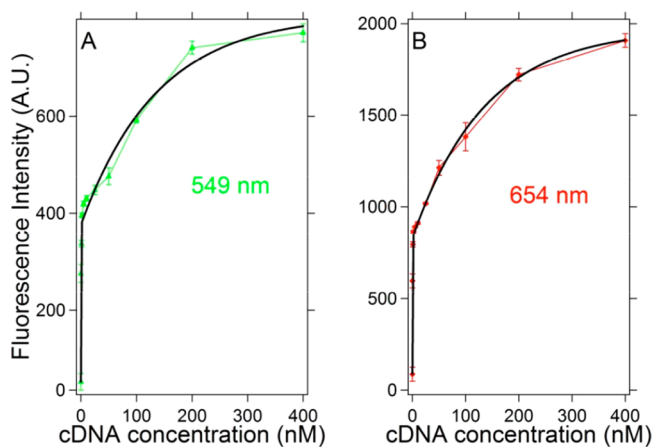

Figure 7. Representation of the maximum fluorescence intensity bands measured at 549 nm (A) and 654 nm (B) of the UCNPs@SiO$_2$-ssDNA nanoparticles as a function of the complementary ssDNA concentration.

Figure 7 shows a trend in the fluorescence intensity upon the addition of the cDNA consisting of two parts. At low concentrations of cDNA (below 2 nM) the fluorescent intensity increases steeply, while in larger concentrations of cDNA there is an additional significant fluorescent increase with a much smaller, saturating slope. This increase is probably due to the gradually larger number of hybridization events near the nanoparticle surface as the concentration of the cDNA is increased.

The fluorescence intensity measured with the highest concentration of cDNA (400 nM) was close to that of the solution of UCNPs@SiO$_2$-ssDNA (0.4 mg/mL) without GO. Thus, we hypothesize that the saturation of the fluorescence intensity at high cDNA concentrations corresponds to a saturation of hybridization events near the nanoparticle surface.

The detection limit of the target sequence for this DNA biosensor was experimentally demonstrated to be at the level of 100 pM. However, the theoretical detection limit inferred from

the double exponential fitting function was 5 pM, limited by the error of the baseline measurement in absence of cDNA. This error was established to be caused by the systematic variation between subsequent recorded spectra. In the excitation arrangement as depicted in Figure 1d, a pencil of light of $\sim20 \times 20 \times 250 \ \mu m^3$ was collected by the spectrometer. Thus, the detection limit of the proposed sensors was 5 pM. This detection limit is lower than other GO−DNA sensors recently published. Thus, for instance, Liu et al.[46] published a GO−DNA sensor based on DNA-functionalized GO and DNA-Au nanoparticles, which showed a detection limit of 200 nM. Luo et al.[47] designed a GO−DNA sensor based on the capacity of GO to inhibit the catalytic activity of the horseradish peroxidase when it was in close contact with the surface of the GO. Thus, by attaching this enzyme to the GO surface by means of a DNA strand, they were able to develop a DNA sensor with a detection limit of 34 pM. Another interesting GO−DNA sensor was designed by Zhao et al.[48] This DNA sensor was based on the use of fluorescent dye-labeled ssDNA strands, which can interact with GO by $\pi-\pi$ stacking interactions. This fact quenched the fluorescence and inhibited the degradation by the exonuclease III, since the physisorbed DNA is not accessible to the enzyme. The hybridization with the complementary DNA not only hampers the dsDNA physisorbtion but also permits their enzymatic degradation and the release of the fluorescent dye, allowing the quantification of target DNA with a detection limit of 20 pM.

The specificity of the sensor was evaluated with a control experiment, in which the UCNPs@SiO$_2$-ssDNA nanoparticles (0.4 mg/mL) were incubated in PBS in the presence of noncomplementary DNA sequences at concentrations from 100 nM to 1 μM. The incubation was performed at 90 °C for 2 min and then a solution of GO in PBS was added obtaining a final concentration of 0.3 mg/mL. The solution was left for 1 h at 40 °C. After cooling down to room temperature, the upconversion fluorescence was measured (see Figure 8).

Figure 8 shows that independently of the concentration of noncomplementary DNA strands, the UCNPs@SiO$_2$-ssDNA fluorescence was quenched by GO. These observations demonstrate the DNA selectivity of the biosensor platform. A schematic illustration of the action mechanism of the sensor is depicted in Scheme 2, which represents the action mechanism
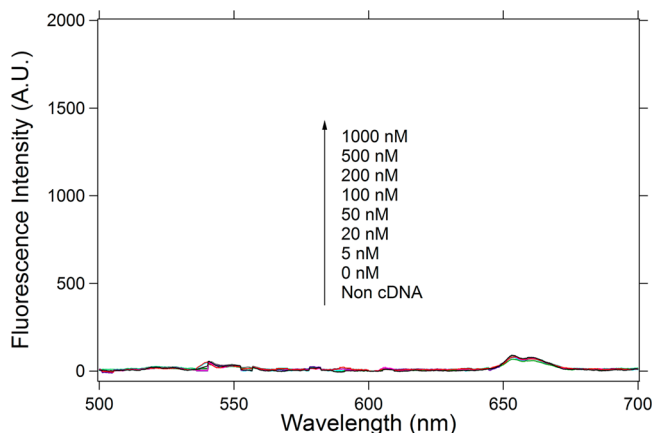

Figure 8. Representation of the upconversion fluorescence spectra of the UCNPs@SiO$_2$-ssDNA nanoparticles (0.4 mg/mL), hybridized at 90 °C for 2 min and at 40 °C for 1 h, with different concentrations of a noncomplementary ssDNA and 0.3 mg/mL of GO (red curves).

Scheme 2. Schematic Representation of the Proposed Sensor Platform under the Presence or Absence of Complementary DNA
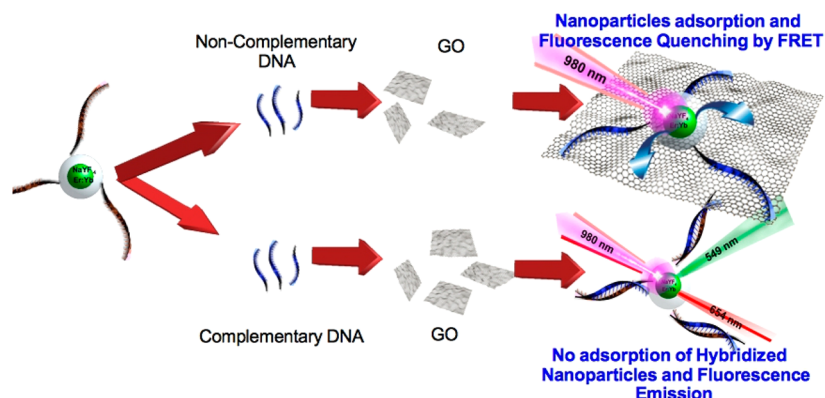
of the DNA sensor platform. In this system the existence of ssDNA on the surface of the UCNPs permits the adsorption of these nanoparticles on the surface of the GO, which leads to the fluorescence quenching of the nanoparticles. In contrast, the presence of complementary DNA produces the hybridization of the ssDNA attached on the surface rendering UCNPs@SiO$_2$-dsDNA, which do not interact with the GO. The lack of interaction maintains the UCNPs@SiO2-dsDNA nanoparticles in dispersion and fluorescent. The fluorescence intensity was demonstrated to be dependent on the number of complementary DNA strands in the medium.

CONCLUSIONS

In this work a DNA biosensor platform was prepared by exploiting the FRET pair formed between UCNPs and GO. The UCNPs were synthesized and functionalized with ssDNA. In the absence of cDNA, the ssDNA-coated UPCNs were physisorbed on the surface of the GO, and their fluorescence was quenched. When the cDNA was present, the UCNPs were not able to physisorb onto the GO template, and thus the fluorescence ability remained unquenched. The fluorescence intensity was correlated to the concentration of cDNA. The detection limit was experimentally shown to be in the picomolar range, which corresponded in our experimental conditions to zeptomoles of cDNA.

ASSOCIATED CONTENT

Ⓢ Supporting Information
Spectra: EDS, FTIR, UV–vis absorption, and fluorescence. This material is available free of charge via the Internet at http://pubs.acs.org.

AUTHOR INFORMATION

Corresponding Authors
*E-mail: bjrubio@ucm.es. (J.R.-R.)
*E-mail: a.kanaras@soton.ac.uk. (A.G.K.)

Notes
The authors declare no competing financial interest.

ACKNOWLEDGMENTS

REFERENCES

(1) Rothemund, P. W. K. Folding DNA to Create Nanoscale Shapes and Patterns. *Nature* **2006**, *440*, 297−302.

(2) He, Y.; Ye, T.; Su, M.; Zhang, C.; Ribbe, A. E.; Jiang, W.; Mao, C. Hierarchical Self-Assembly of DNA into Symmetric Supramolecular Polyhedra. *Nature* **2008**, *452*, 198−201.

(3) Yan, H.; Zhang, X.; Shen, Z.; Seeman, N. C. A Robust DNA Mechanical Device Controlled by Hybridization Topology. *Nature* **2002**, *415*, 62−65.

(4) Le, J. D.; Pinto, Y.; Seeman, N. C.; Musier-Forsyth, K.; Taton, A. T.; Kiehl, R. A. DNA-Templated Self-Assembly of Metallic Nano-component Arrays on a Surface. *Nano Lett.* **2004**, *4* (12), 2343−2347.

(5) Zhang, J.; Liu, Y.; Ke, Y.; Yan, H. Periodic Square-Like Gold Nanoparticle Arrays Templated by Self-Assembled 2D DNA Nanogrids on a Surface. *Nano Lett.* **2006**, *6* (2), 248−251.

(6) Ding, B.; Deng, Z.; Yan, H.; Cabrini, S.; Zuckermann, R. N.; Bokor, J. Gold Nanoparticle Self-Similar Chain Structure Organized by DNA Origami. *J. Am. Chem. Soc.* **2010**, *132*, 3248−3249.

(7) Niemeyer, C. M.; Adler, M. Nanomechanical Devices Based on DNA. *Angew. Chem., Int. Ed.* **2002**, *41* (20), 3779−3783.

(8) Wang, J.; Cai, X.; Rivas, G.; Shiraishi, H.; Farias, P. A. M.; Dontha, N. DNA Electrochemical Biosensor for the Detection of Short DNA Sequences Related to the Human Immunodeficiency Virus. *Anal. Chem.* **1996**, *68*, 2629−2634.

(9) Mao, X.; Yang, L.; Su, X. L.; Li, Y. A Nanoparticle Amplification Based Quartz Crystal Microbalance DNA Sensor for Detection of Escherichia coli O157:H7. *Biosens. Bioelectron.* **2006**, *21*, 1178−1185.

(10) Liu, G.; Wan, Y.; Gau, V.; Zhang, J.; Wang, L.; Song, S.; Fan, C. An Enzyme-Based E-DNA Sensor for Sequence-Specific Detection of Femtomolar DNA Targets. *J. Am. Chem. Soc.* **2008**, *130*, 6820−6825.

(11) Marrazza, G.; Chiti, G.; Mascini, M.; Anichini, M. Detection of Human Apolipoprotein E Genotypes by DNA Electrochemical Biosensor Coupled with PCR. *Clin. Chem.* **2000**, *46* (1), 31−37.

(12) Zhang, X. B.; Wang, Z.; Xing, H.; Xiang, Y.; Lu, Y. Catalytic and Molecular Beacons for Amplified Detection of Metal Ions and Oganic Molecules with High Sensitivity. *Anal. Chem.* **2010**, *82*, 5005−5011.

(13) Liu, X.; Tan, W. A Fiber-Optic Evanescent Wave DNA Biosensor Based on Novel Molecular Beacons. *Anal. Chem.* **1999**, *71*, 5054−5059.

(14) Nutiu, R.; Li, Y. Structure-Switching Signaling Aptamers. *J. Am. Chem. Soc.* **2003**, *125*, 4771−4778.

(15) Du, H.; Disney, M. D.; Miller, B. L.; Krauss, T. D. Hybridization-Based Unquenching of DNA Hairpins on Au Surfaces: Prototypical "Molecular-Beacon" Biosensors. *J. Am. Chem. Soc.* **2003**, *125*, 4012−4013.

(16) Bonnet, G.; Krichevsky, O.; Libchaber, A. Kinetics of Conformational Fluctuations in DNA Hairpin-Loops. *Proc. Natl. Acad. Sci. U. S. A.* **1998**, *95*, 8602−8606.

(17) Zhang, J.; Qi, H.; Li, Y.; Yang, J.; Gao, Q.; Zhang, C. Electrogenerated Chemiluminescence DNA Biosensor Based on Hairpin DNA Probe Labeled with Ruthenium Complex. *Anal. Chem.* **2008**, *80*, 2888−2894.

(18) Suzuki, M.; Husimi, Y.; Komatsu, H.; Suzuki, K.; Douglas, K. T. Quantum Dot FRET Biosensors that Respond to pH, to Proteolytic or Nucleolytic Cleavage, to DNA Synthesis, or to a Multiplexing Combination. *J. Am. Chem. Soc.* **2008**, *130*, 5720−5725.

(19) Chen, Z.; Chen, H.; Hu, H.; Yu, M.; Li, F.; Zhang, Q.; Zhou, Z.; Yi, T.; Huang, C. Versatile Synthesis Strategy for Carboxylic Acid-Functionalized Upconverting Nanophosphors as Biological Labels. *J. Am. Chem. Soc.* **2008**, *130*, 3023−3029.

(20) Frangioni, J. V. In Vivo Near-Infrared Fluorescence Imaging. *Curr. Opin. Chem. Biol.* **2003**, *7*, 626−634.

(21) Liu, J.; Liu, Y.; Bu, W.; Bu, J.; Sun, Y.; Du, J.; Shi, J. Ultrasensitive Nanosensors Based on Upconversion Nanoparticles for Selective Hypoxia Imaging in Vivo upon Near-Infrared Excitation. *J. Am. Chem. Soc.* **2014**, *136*, 9701−9709.

(22) Binnemans, K. Lanthanide-Based Luminescent Hybrid Materials. *Chem. Rev.* **2009**, *109*, 4283−4374.

(23) Chen, F.; Bu, W.; Zhang, S.; Liu, J.; Fan, W.; Zhou, L.; Peng, W.; Shi, J. Gd^{3+}-Ion-Doped Upconversion Nanoprobes: Relaxivity Mechanism Probing and Sensitivity Optimization. *Adv. Funct. Mater.* **2012**, *23* (3), 298−307.

(24) Xu, C. T.; Svenmarker, P.; Liu, H.; Wu, X.; Messing, M. E.; Wallenberg, L. R.; Andersson-Engels, S. High-Resolution Fluorescence Diffuse Optical Tomography Developed with Nonlinear Upconverting Nanoparticles. *ACS Nano* **2012**, *6* (6), 4788−4795.

(25) Wang, Y. F.; Liu, G. Y.; Sun, L. D.; Xiao, J. W.; Zhou, J. C.; Yan, C. H. Nd^{3+}-Sensitized Upconversion Nanophosphors: Efficient In Vivo Bioimaging Probes with Minimized Heating Effect. *ACS Nano* **2013**, *7* (8), 7200−7206.

(26) Yan, B.; Boyer, J. C.; Habault, D.; Branda, N. R.; Zhao, Y. Near Infrared Light Triggered Release of Biomacromolecules from Hydrogels Loaded with Upconversion Nanoparticles. *J. Am. Chem. Soc.* **2012**, *134*, 16558−16561.

(27) Chen, G.; Qiu, H.; Prasad, P. N.; Chen, X. Upconversion Nanoparticles: Design, Nanochemistry, and Applications in Theranostics. *Chem. Rev.* **2014**, *114*, 5161−5214.

(28) Chatterjee, D. K.; Rufaihah, A. J.; Zhang, Y. Upconversion Fluorescence Imaging of Cells and Small Animals Using Lanthanide Doped Nanocrystals. *Biomaterials* **2008**, *29*, 937−943.

(29) Huang, X.; El-Sayed, I. H.; Qian, W.; El-Sayed, M. A. Cancer Cell Imaging and Photothermal Therapy in the Near-Infrared Region by Using Gold Nanorods. *J. Am. Chem. Soc.* **2006**, *128*, 2115−2120.

(30) Li, Z.; Zhang, Y.; Jiang, S. Multicolor Core/Shell-Structured Upconversion Fluorescent Nanoparticles. *Adv. Mater.* **2008**, *20*, 4765−4769.

(31) Zhang, H.; Li, Y.; Ivanov, I. A.; Qu, Y.; Huang, Y.; Duan, X. Plasmonic Modulation of the Upconversion Fluorescence in $NaYF_4$:Yb/Tm Hexaplate Nanocrystals Using Gold Nanoparticles or Nanoshells. *Angew. Chem., Int. Ed.* **2010**, *122*, 2927−2930.

(32) Rantanen, T.; Järvenpää, M. L.; Vuojola, J.; Kuningas, K.; Soukka, T. Fluorescence-Quenching-Based Enzyme-Activity Assay by Using Photon Upconversion. *Angew. Chem., Int. Ed.* **2008**, *47*, 3811−3813.

(33) Li, Z.; Wang, L.; Wang, Z.; Liu, X.; Xiong, Y. Modification of $NaYF_4$:Yb,Er@SiO_2 Nanoparticles with Gold Nanocrystals for Tunable Green-to-Red Upconversion Emissions. *J. Phys. Chem. C* **2011**, *115*, 3291−3296.

(34) Wu, T.; Wilson, D.; Branda, N. R. Fluorescent Quenching of Lanthanide-Doped Upconverting Nanoparticles by Photoresponsive Polymer Shells. *Chem. Mater.* **2014**, *26*, 4313−4320.

(35) Liu, C.; Wang, Z.; Jia, H.; Li, Z. Efficient Fluorescence Resonance Energy Transfer between Upconversion Nanophosphors and Graphene Oxide: a Highly Sensitive Biosensing Platform. *Chem. Commun.* **2011**, *47*, 4661−4663.

(36) Wang, Y.; Li, Z.; Hu, D.; Lin, C. T.; Li, J.; Li, Y. Aptamer/Graphene Oxide Nanocomplex for In Situ Molecular Probing in Living Cells. *J. Am. Chem. Soc.* **2010**, *132*, 9274−9276.

(37) Liu, C.; Wang, H.; Li, X.; Chen, D. Monodisperse, Size Tunable and Highly Efficient β-NaYF$_4$:Yb,Er(Tm) Up-Conversion Luminescent Nanospheres: Controllable Synthesis and Their Surface Modifications. *J. Mater. Chem.* **2009**, *19*, 3546−3553.

(38) Li, Z.; Zhang, Y. An Efficient and User-Friendly Method for the Synthesis of Hexagonal-Phase $NaYF_4$:Yb,Er/Tm Nanocrystals with Controllable Shape and Upconversion Fluorescence. *Nanotechnology* **2008**, *19*, 345606−345611.

(39) Qian, H. S.; Guo, H. C.; Ho, P. C. L.; Mahendran, R.; Zhang, Y. Mesoporous-Silica-Coated Up-Conversion Fluorescent Nanoparticles for Photodynamic Therapy. *Small* **2009**, *20* (5), 2285−2290.

(40) Han, Y.; Jiang, J.; Lee, S. S.; Ying, J. Y. Reverse Microemulsion-Mediated Synthesis of Silica-Coated Gold and Silver Nanoparticles. *Langmuir* **2008**, *24*, 5842−5848.

(41) Serrano-Ruiz, D.; Alonso-Cristobal, P.; Mendez-Gonzalez, D.; Laurenti, M.; Olivero-David, R.; Lopez-Cabarcos, E.; Rubio-Retama, J. Nanosegregated Polymeric Domains on the Surface of Fe_3O_4@SiO_2 Particles. *J. Polym. Sci., Part A: Polym. Chem.* **2014**, *52*, 2966−2975.

(42) Vaz, A. M.; Serrano-Ruiz, D.; Laurenti, M.; Alonso-Cristobal, P.; Lopez-Cabarcos, E.; Rubio-Retama, J. Synthesis and Characterization of Biocatalytic γ-Fe$_2$O$_3$@SiO_2 Particles as Recoverable Bioreactors. *Colloids Surf., B* **2014**, *114*, 11−19.

(43) Yi, G.; Sun, B.; yang, F.; Chen, D.; Zhou, Y.; Cheng, J. Synthesis and Characterization of High-Efficiency Nanocrystal Up-Conversion Phosphors: Ytterbium and Erbium Codoped Lanthanum Molybdate. *Chem. Mater.* **2002**, *14*, 2910−2914.

(44) Boyer, J.-C.; van Veggel, F. J. C. M. Absolute Quantum Yield Measurements of Colloidal $NaYF_4$:Er^{3+},Yb^{3+} Upconverting Nanoparticles. *Nanoscale* **2010**, *2*, 1417−1419.

(45) Bartczak, D.; Kanaras, A. G. Preparation of Peptide Functionalized Gold Nanoparticles Using One Pot EDC/sulfo-NHS Coupling. *Langmuir* **2011**, *27* (16), 10119−10123.

(46) Liu, F.; Choi, J. Y.; Seo, T. S. Graphene Oxide Arrays for Detecting Specific DNA Hybridization by Fluorescence Resonance Energy Transfer. *Biosens. Bioelectron.* **2010**, *25*, 2361−2365.

(47) Luo, M.; Chen, X.; Zhou, G.; Xiang, X.; Chen, L.; Ji, X.; He, Z. Chemiluminescence Biosensors for DNA Detection Using Graphene Oxide and a Horseradish Peroxidase-mimicking DNAzyme. *Chem. Commun.* **2012**, *48*, 1126−1128.

(48) Zhao, H. X.; Ma, Q. J.; Wu, X. X.; Zhu, Z. Graphene Oxide-based Biosensor for Sensitive Fluorescence Detection of DNA Based on Exonuclease III-Aided Signal Amplification. *Anal. Chim. Acta* **2012**, *740*, 88−92.